

Stellar Occultation by Comet 67P/Churyumov-Gerasimenko Observed with
Rosetta's Alice Far-Ultraviolet Spectrograph

BRIAN A. KEENEY,¹ S. ALAN STERN,¹ PAUL D. FELDMAN,² MICHAEL F. A'HEARN,^{3,*} JEAN-LOUP BERTAUX,⁴
LORI M. FEAGA,³ MATTHEW M. KNIGHT,³ RICHARD A. MEDINA,¹ JOHN NOONAN,⁵ JOEL WM. PARKER,¹
JON P. PINEAU,⁶ REBECCA N. SCHINDHELM,^{1,7} ANDREW J. STEFFL,¹ M. VERSTEEG,⁸ RONALD J. VERVACK, JR.,⁹ AND
HAROLD A. WEAVER⁹

¹*Southwest Research Institute, Department of Space Studies, Suite 300, 1050 Walnut St., Boulder, CO 80302, USA; bkeeney@gmail.com*

²*Department of Physics and Astronomy, Johns Hopkins University, 3400 N. Charles St., Baltimore, MD 21218, USA*

³*Department of Astronomy, University of Maryland, College Park, MD 20742, USA*

⁴*LATMOS, CNRS/UVSQ/IPSL, 11 Boulevard d'Alembert, F-78280 Guyancourt, France*

⁵*Lunar and Planetary Laboratory, University of Arizona, 1629 E. University Blvd., Tucson, AZ 85721, USA*

⁶*Stellar Solutions, Inc., 250 Cambridge Ave., Suite 204, Palo Alto, CA 94306, USA*

⁷*Ball Aerospace and Technology Corp., 1600 Commerce St., Boulder, CO 80301, USA*

⁸*Southwest Research Institute, 6220 Culebra Rd., San Antonio, TX 78238, USA*

⁹*Space Exploration Sector, Johns Hopkins University Applied Physics Laboratory, 11100 Johns Hopkins Rd., Laurel, MD 20723, USA*

(Received 2018 November 8; Revised 2019 February 25; Accepted 2019 March 15)

Submitted to AJ

ABSTRACT

Following our previous detection of ubiquitous H₂O and O₂ absorption against the far-UV continuum of stars located near the nucleus of Comet 67P/Churyumov-Gerasimenko, we present a serendipitously observed stellar occultation that occurred on 2015 September 13, approximately one month after the comet's perihelion passage. The occultation appears in two consecutive 10-minute spectral images obtained by Alice, *Rosetta*'s ultraviolet (700-2100 Å) spectrograph, both of which show H₂O absorption with column density > 10^{17.5} cm⁻² and significant O₂ absorption (O₂/H₂O ≈ 5-10%). Because the projected distance from the star to the nucleus changes between exposures, our ability to study the H₂O column density profile near the nucleus (impact parameters < 1 km) is unmatched by our previous observations. We find that the H₂O and O₂ column densities decrease with increasing impact parameter, in accordance with expectations, but the O₂ column decreases ~ 3 times more quickly than H₂O. When combined with previously published results from stellar appulses, we conclude that the O₂ and H₂O column densities are highly correlated, and O₂/H₂O decreases with increasing H₂O column.

Keywords: comets: individual (67P) – ultraviolet: planetary systems

1. INTRODUCTION

The double-focusing mass spectrometer (DFMS) of the *Rosetta* Orbiter Spectrometer for Ion and Neutral Analysis (ROSINA; Balsiger et al. 2007) has found that O₂ is the fourth most abundant parent species in the coma of Comet 67P/Churyumov-Gerasimenko (67P/C-G), behind only H₂O, CO₂, and CO (Le Roy et al. 2015; Fougere et al. 2016). The ubiquitous, abundant presence of O₂ was surprising since it had never been detected in a comet before (Bieler et al. 2015).

Feldman et al. (2016) confirmed the presence of substantial O₂ in the coma of 67P/C-G during gaseous outbursts with Alice, *Rosetta*'s ultraviolet spectrograph (Stern et al. 2007). Later, Keeney et al. (2017) directly detected O₂ absorption in Alice data using stellar sight lines temporarily projected near the nucleus (“stellar appulses”). These sight lines were observed over a wide range of heliocentric distances (1.2-2.3 AU) and impact parameters (4-20 km), yielding log $N_{\text{H}_2\text{O}} = 15.2-17.1$ (all column densities, N , herein are quoted in units of cm⁻²) and a median value of $N_{\text{O}_2}/N_{\text{H}_2\text{O}} = 25\%$.

Several *Rosetta* instruments can directly detect H₂O in the coma of 67P/C-G: Alice, ROSINA, the Visible

* Deceased

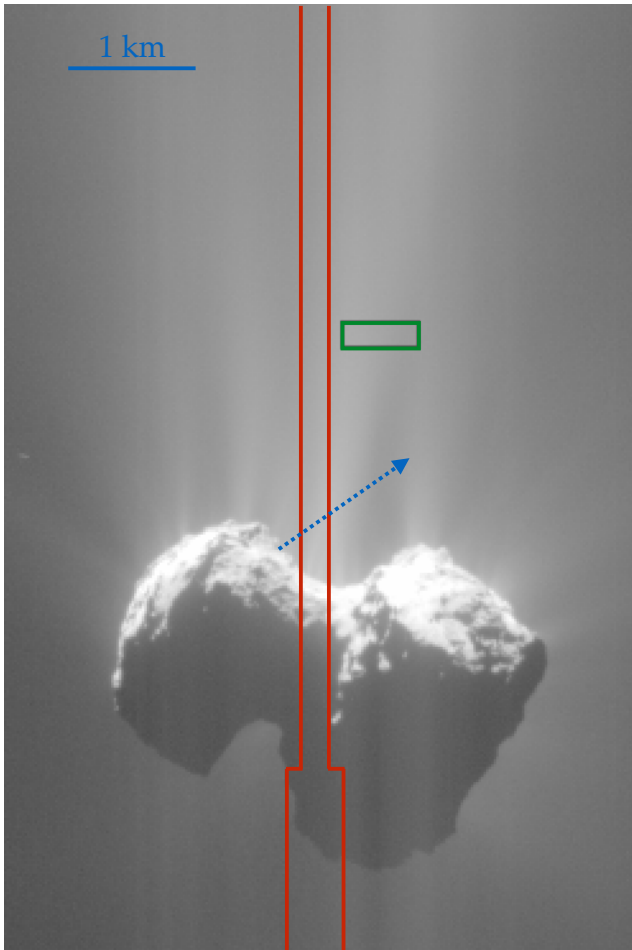


Figure 1. Subsection of a NAVCAM image taken while HD 4150 was occulted by 67P/C-G, ~ 20 minutes before the star entered the Alice slit (red). The VIRTIS-H aperture is shown in green, and the approximate path of HD 4150 through the Alice slit is shown by a dashed blue arrow. The image is oriented such that the Sun is toward the top, and the field-of-view is $\sim 1^\circ \times 1.5^\circ$ ($\sim 5 \times 7.5 \text{ km}^2$).

and Infrared Thermal Imaging Spectrometer (VIRTIS; Coradini et al. 2007), and the Microwave Instrument for the *Rosetta* Orbiter (MIRO; Gulkis et al. 2007). All but ROSINA are remote-sensing instruments that measure or infer column densities along a line of sight, and $N_{\text{H}_2\text{O}}$ measured by Alice (Keeney et al. 2017) agrees with VIRTIS values near perihelion (Bockelée-Morvan et al. 2016). However, only Alice and ROSINA can directly detect O_2 , and the relative abundance of $\text{O}_2/\text{H}_2\text{O}$ in the Alice data was nearly an order of magnitude larger than the average ROSINA value ($n_{\text{O}_2}/n_{\text{H}_2\text{O}} = 3.85 \pm 0.85\%$; Bieler et al. 2015, where n is number density measured at the spacecraft position). The consistency in $N_{\text{H}_2\text{O}}$ between Alice and VIRTIS suggests that the methodology of Keeney et al. (2017) is trustworthy, but the discrepancy in $\text{O}_2/\text{H}_2\text{O}$ remains puzzling.

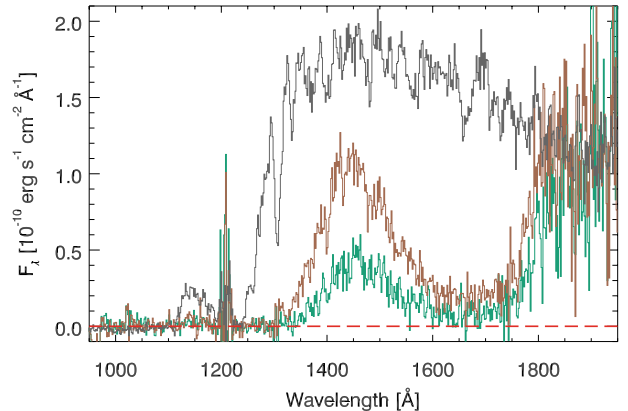


Figure 2. Three spectra of HD 4150 obtained by Alice. The revisit (i.e., intrinsic) spectrum taken on 2016 June 6 is shown in gray, and the post-occultation spectra taken on 2015 September 13 at 13:52:04 and 14:02:49 UT are shown in green and brown, respectively.

Here we present a stellar occultation by 67P/C-G observed with Alice. We describe our observations in Section 2, and our analysis procedure in Section 3. Section 4 compares the H_2O and O_2 column densities for our stellar occultation with those of Keeney et al. (2017) and ROSINA measurements (Bieler et al. 2015; Hansen et al. 2016), and Section 5 summarizes our main findings.

2. OBSERVATIONS

The A0 IV star HD 4150 was occulted by 67P/C-G on 2015 September 13, approximately one month after the comet’s perihelion passage. The occultation was serendipitously observed by Alice during the course of normal operations. During this phase of the mission, Alice was integrating nearly continuously to catalog emissions from the near-nucleus coma (Pineau et al. 2019).

Figure 1 shows a $\sim 5 \times 7.5 \text{ km}^2$ subsection of a *Rosetta* navigation camera (NAVCAM) image taken at 13:36:02 UT, while HD 4150 was occulted by 67P/C-G and ~ 20 minutes before it entered the Alice slit. The Alice slit is $5^\circ 5'$ long and has a dog-bone shape that is twice as wide at the top and bottom as in the center (Stern et al. 2007); its position with respect to the nucleus is shown in red in Figure 1, and the transition between the wide-bottom and narrow-center regions of the slit is evident. Figure 1 also shows the approximate path of HD 4150 as it emerges from behind the small lobe of 67P/C-G and crosses the Alice slit from left to right at an angle of $\sim 35^\circ$ over the “neck” of the nucleus.

HD 4150 appears in two consecutive 10-minute spectral images with start times of 13:52:04 and 14:02:49 UT, respectively. For the first five minutes of the first exposure, the star is occulted by the comet nucleus. The star remains in the Alice slit for the remainder of the first ex-

posure and the first five minutes of the second exposure. During these exposures, 67P/C-G was 1.30 AU from the Sun, *Rosetta* was orbiting 313 km from the comet center, and the solar phase angle was 108° .

The spectra of HD 4150 extracted from these exposures are shown in green (first exposure) and brown (second exposure) in Figure 2. The observed stellar fluxes are corrected for the reduced amount of time the star was in the slit during these exposures. Nevertheless, differences between the two exposures are evident; most notably, the first (green) spectrum has less flux from 1350-1600 Å.

HD 4150 was re-observed (“revisited”) on 2016 June 6 when it was far from the nucleus, at an off-nadir angle of 79° . The purpose of this 15-minute integration, which started at 06:02:24 UT, was to characterize the intrinsic stellar spectrum without the presence of foreground coma absorption (see Keeney et al. 2017 for details). When HD 4150 was revisited, the comet was 3.15 AU from the Sun and the solar phase angle was 67° . The intrinsic stellar spectrum is shown in gray in Figure 2, and has considerably more flux from 1250-1800 Å than the spectra obtained immediately after the occultation.

The analysis below, and that of Keeney et al. (2017), assumes that the stellar spectrum obtained when the star was revisited while far from the nucleus is equivalent to the intrinsic stellar spectrum (i.e., that there is no foreground coma absorption at that time). Although it is true that O_2 is extremely volatile, with a sublimation temperature in vacuum of ~ 30 K (Fray & Schmitt 2009), it has been found to be strongly correlated with H_2O in the coma of 67P/C-G (Bieler et al. 2015; Fougere et al. 2016), and the production rate of H_2O was down by 2-3 orders of magnitude at 3.15 AU compared to 1.30 AU (Hansen et al. 2016; Gasc et al. 2017). However, even if our assumptions are incorrect and a small amount of foreground coma absorption is present in the revisit spectrum, then this would cause us to *underestimate* the amount of foreground coma absorption at the time of the occultation¹.

3. RESULTS AND ANALYSIS

The spectra of HD 4150 taken immediately after the occultation by 67P/C-G were analyzed analogously to the stellar appulse spectra of Keeney et al. (2017), except in one regard. The UV-bright stars that Keeney et al. (2017) used to study the near-nucleus coma all had measurable far-UV flux down to ~ 900 Å (see Figure 1 of Keeney et al. 2017), but HD 4150 is an A0 star with

almost no flux below ~ 1250 Å (see Figure 2). This lack of flux blueward of 1250 Å has important consequences for our analysis.

Although H_2O and O_2 have relatively large cross sections from 1250-1800 Å (Chung et al. 2001; Yoshino et al. 2005), other abundant coma species do not (i.e., CO and CO_2 ; Cairns & Samson 1965; Yoshino et al. 1996), which means that they cannot be directly constrained by our data. Fortunately, at the time of the occultation VIRTIS was acquiring data while pointed ~ 3.6 km above the sunward limb of the nucleus. Thus, we adopt their contemporaneous column density ratio of $N_{CO_2}/N_{H_2O} = 0.310 \pm 0.034$ (Bockelée-Morvan et al. 2016) for our analysis. The position of the VIRTIS-H aperture with respect to the Alice slit and the path of HD 4150 are shown in Figure 1.

To isolate the coma signature from the intrinsic stellar flux and interstellar absorption, we divided the stellar spectra taken immediately post-occultation (i.e., the green and brown spectra in Figure 2) by the spectrum of the star taken much later (i.e., the gray spectrum in Figure 2), after first scaling them to have the same median flux from 1850-1950 Å. This procedure reduces our sensitivity to the uncertainty in the amount of time the star was in the slit during our long exposures (Keeney et al. 2017). The resulting normalized spectrum quantifies the amount of foreground coma absorption in the post-occultation exposures.

Keeney et al. (2017) modeled far-UV absorption from ten molecular species (see their Table 3 and Figure 2 for adopted cross sections) in Alice spectra normalized as above. We use the same procedure here, except that we only fit wavelengths in the range 1250-1950 Å because HD 4150 has insufficient flux blueward of 1250 Å (see Figure 2). Consequently, we remove CO from our fits because it has no appreciable cross section redward of 1050 Å (Cairns & Samson 1965).

The column density of H_2O is fit directly and allowed to vary in the range $\log N_{H_2O} = 14-18$. The abundances of all other species are fit relative to N_{H_2O} ; O_2 is allowed to vary in the range $N_{O_2}/N_{H_2O} = 0-1$, CO_2 is fixed at the ratio measured by VIRTIS ($N_{CO_2}/N_{H_2O} = 0.310 \pm 0.034$; Bockelée-Morvan et al. 2016), and all other species (CH_4 , C_2H_2 , C_2H_6 , C_2H_4 , C_4H_2 , and H_2CO) are constrained to have $N/N_{H_2O} < 0.01$ (Le Roy et al. 2015). All species except CO and CO_2 are treated the same as they were in Keeney et al. (2017). The absorption profiles are determined directly from high-resolution cross sections (1-2 Å for H_2O and O_2 ; references for all adopted cross sections are listed in Table 3 of Keeney et al. 2017), then convolved to the spectral

¹ The same can be said for the stellar appulse analysis of Keeney et al. (2017).

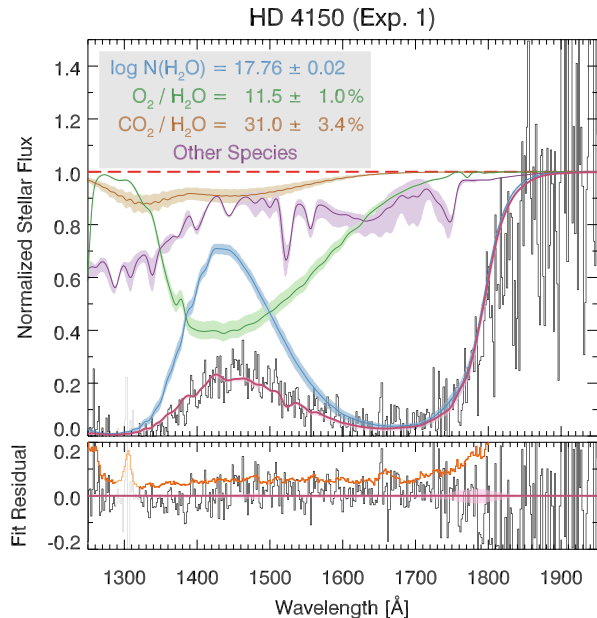


Figure 3. Best-fit column densities for the first post-occultation exposure of HD 4150, with 95% (2σ) confidence bands. *Top:* the normalized stellar flux with ensemble fit (pink) and individual-species absorption overlaid. *Bottom:* the residual of the ensemble fit with 1σ flux uncertainty (orange) overlaid. Masked regions are shown in lighter hues in both panels; these regions are not used to constrain the fits.

resolution of Alice (9 Å FWHM for the narrow part of the slit) before being compared to the data.

Our fits to the spectra of HD 4150 taken immediately after its occultation by 67P/C-G are shown in Figure 3-4. The top panels show the normalized spectra in black, and our best-fit absorption profiles from H₂O (blue), O₂ (green), CO₂ (brown), and all other species (purple). The ensemble fit from all species is shown in pink, and the shaded regions represent 95% (2σ) confidence bands. Recall that $N_{\text{CO}_2}/N_{\text{H}_2\text{O}}$ is held fixed at the value measured contemporaneously by VIRTIS (Bockelée-Morvan et al. 2016). The bottom panel shows the residual of the ensemble fit as a function of wavelength, with 1σ flux uncertainty overlaid in orange. Masked regions that are not used to constrain the fits are shown in lighter hues in both panels.

We searched for systematic offsets in the best-fit H₂O and O₂ column densities using Monte Carlo simulations to compare the values retrieved from forward-modeled data with Poissonian noise and known input values. However, unlike in Keeney et al. (2017), we found no evidence for systematic offsets. Reassuringly, the large optical depth of the H₂O absorption makes the fitting results more robust. Thus, we adopt the H₂O and O₂ column densities returned by our fits as final.

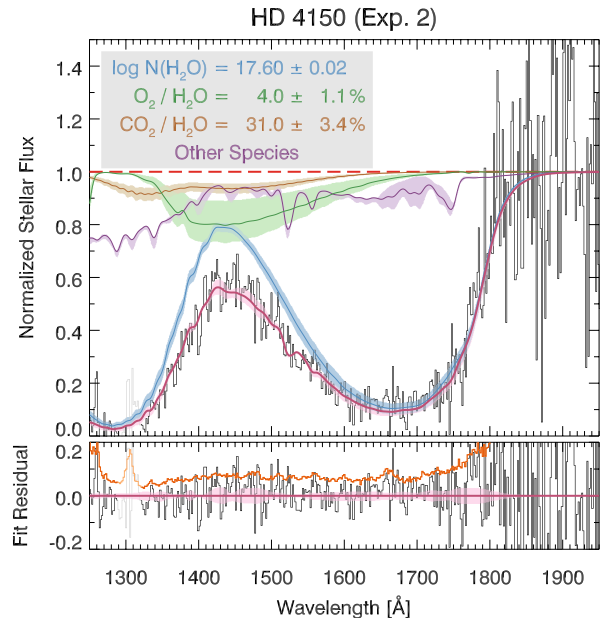


Figure 4. Best-fit column densities for the second post-occultation exposure of HD 4150, with 95% (2σ) confidence bands.

4. DISCUSSION

The decrease in the H₂O column density from the first exposure of HD 4150 to the second (see Figure 3-4) agrees with the naïve expectation that $N \propto \rho^{-1}$ (Haser 1957), where ρ is the impact parameter with respect to the nucleus. $N_{\text{H}_2\text{O}}$ decreases by a factor of ~ 1.4 between the two exposures when ρ increases by a factor of ~ 1.3 (we estimate $\rho \approx 0.3$ km and 0.4 km for the first and second exposures, respectively; see Figure 1). However, the contemporaneous VIRTIS measurement ($\log N_{\text{H}_2\text{O}} = 17.00 \pm 0.04$ at $\rho \approx 2.7$ km; Bockelée-Morvan et al. 2016)² is not as consistent with $N \propto \rho^{-1}$, finding a factor of ~ 6 decrease in $N_{\text{H}_2\text{O}}$ compared to the first post-occultation exposure when ρ increases by a factor of ~ 9 .

Of course, the Haser (1957) model, which assumes spherically symmetric outflow from a point source, is far too simplistic to be directly applied to data from Rosetta 67P/C-G. From Rosetta’s vantage point embedded in the coma of 67P/C-G, the nucleus is clearly resolved and far from spherical (Figure 1), and observed gas (e.g., Migliorini et al. 2016) and dust (e.g., Gerig et al. 2018) outbursts are not axisymmetric. Thus, it

² Bockelée-Morvan et al. (2016) list $\rho = 3.6$ km for the contemporaneous exposure, which is measured from the center of the nucleus. The value we list is measured with respect to the limb of the nucleus for consistency with Figure 1.

is questionable whether the analytic prediction of *Haser* (1957, namely, $N \propto \rho^{-1}$) holds for Alice data.

The best-fit values of the O_2 column density are $\log N_{O_2} = 16.82 \pm 0.04$ for the first post-occultation exposure (Figure 3) and $\log N_{O_2} = 16.20 \pm 0.12$ for the second exposure (Figure 4), corresponding to a factor of ~ 4 decrease. It is unclear why N_{O_2} is decreasing almost three times more quickly than N_{H_2O} . Keeney et al. (2017) found no clear trend in N_{O_2} as a function of impact parameter when $\rho \approx 5\text{--}15$ km (see their Figure 9). However, the exposures of HD 4150 probe the coma much closer to the nucleus than any of our previous sight lines, so we cannot confidently extrapolate the Keeney et al. (2017) measurements to $\rho < 1$ km.

The most puzzling result of Keeney et al. (2017) was that the relative abundance of O_2 with respect to H_2O inferred from Alice data (median $N_{O_2}/N_{H_2O} = 25\%$) was nearly an order of magnitude larger than the average value of $n_{O_2}/n_{H_2O} = 3.85 \pm 0.85\%$ found by ROSINA (Bieler et al. 2015). In fact, the datasets almost seemed to be mutually exclusive; Keeney et al. (2017) did not find a single high-quality example with $N_{O_2}/N_{H_2O} < 10\%$ (although there were several upper limits), and ROSINA almost never measured $n_{O_2}/n_{H_2O} > 10\%$ (Bieler et al. 2015; Fougere et al. 2016). Keeney et al. (2017) speculated that the discrepancy could be attributed to comparing column density along a line of sight near the nucleus with number density measured *in situ* at the spacecraft position, but no firm conclusions could be drawn. It is therefore reassuring that we measure a relative abundance of O_2/H_2O that is nearly identical to the average ROSINA value in one of the post-occultation exposures (see Figure 4).

However, whereas Keeney et al. (2017) did not find any instances of O_2/H_2O consistent with ROSINA measurements in absorption, the emission-line technique of Feldman et al. (2016) frequently infers O_2/H_2O values near the sunward limb of the nucleus in Alice data that are consistent with ROSINA values. For example, an estimate of O_2/H_2O can be derived from exposures taken just before and just after the occultation using the ratio of the semi-forbidden O I] 1356 Å line to H I Lyβ. If we assume that all of the O I] 1356 Å emission near the limb comes from electron impact on H_2O (Makarov et al. 2004), O_2 (Kanik et al. 2003), and CO_2 (Mumma et al. 1972) at an energy of 100 eV, then the brightness of the C I 1657 Å line suggests that 25–30% of the 1356 Å brightness comes from electron impact dissociation of CO_2 . Similarly, large off-nadir steps along the slit suggest that 25–30% of the H I Lyβ brightness comes from resonant scattering in the coma. After these corrections, we estimate that $O_2/H_2O \approx 4\%$ in the Alice exposures

surrounding the occultation. Although this estimate is predicated on many assumptions, it is nevertheless reassuring that it is identical to the value we derived for our second exposure (see Figure 4).

Further, the above estimate is consistent with $O_2/H_2O \approx 4\%$ being the quiescent value at this time, whereas the elevated value of $O_2/H_2O \approx 10\%$ (Figure 3) may be associated with a strong, collimated dust outburst observed in the sunward direction by VIRTIS-H (Bockelée-Morvan et al. 2017) and VIRTIS-M (Rinaldi et al. 2018). The dust outburst peaked at approximately 13:30:00 UT (Rinaldi et al. 2018), ~ 20 minutes before our first post-occultation exposure began. At the beginning of the first Alice exposure, the radiance of the dust emission had decayed to $\sim 20\%$ of its peak compared to the quiescent level, and by the beginning of the second Alice exposure it had returned to the quiescent level altogether (see Figure 4 of Rinaldi et al. 2018). Thus, one plausible explanation for the differing O_2/H_2O levels in the two Alice exposures is a non-constant production rate of O_2 (i.e., the amount of O_2 in the first exposure is affected by the dust outburst). However, Bockelée-Morvan et al. (2017) found no increase in H_2O or CO_2 column density during the outburst, so it is unclear why the O_2 production rate would be affected but not those of H_2O and CO_2 .

Figure 5 shows N_{O_2} and N_{O_2}/N_{H_2O} as a function of N_{H_2O} for the two post-occultation exposures of HD 4150 and the stellar appulses of Keeney et al. (2017). We confirm that N_{O_2} and N_{H_2O} are strongly correlated as expected due to the strong correlation between n_{O_2} and n_{H_2O} in ROSINA data (Bieler et al. 2015; Fougere et al. 2016). Owing to the smaller impact parameters probed, our occultation data find larger N_{H_2O} values and smaller N_{O_2}/N_{H_2O} than the appulses, and overall there is a clear trend of decreasing O_2/H_2O with increasing N_{H_2O} in Alice data (e.g., when $N_{H_2O} < 10^{16}$ cm $^{-2}$ the median $N_{O_2}/N_{H_2O} = 41\%$, whereas the median $N_{O_2}/N_{H_2O} = 16\%$ for larger N_{H_2O}).

This trend, which was first noted by Bieler et al. (2015), suggests that we are able to detect an O_2/H_2O abundance consistent with the ROSINA measurements in Figure 4 simply because the H_2O column density is sufficiently large. A S/N-dependent detection threshold for N_{O_2} in Alice data is consistent with this trend, but we see no clear evidence that our measurements are strongly affected by such a selection bias (Figure 5). Further, this hypothesis cannot explain **all** of the Alice measurements since Keeney et al. (2017) found two examples where $N_{O_2}/N_{H_2O} > 40\%$ when $N_{H_2O} > 10^{16}$ cm $^{-2}$. Thus, a full explanation for the

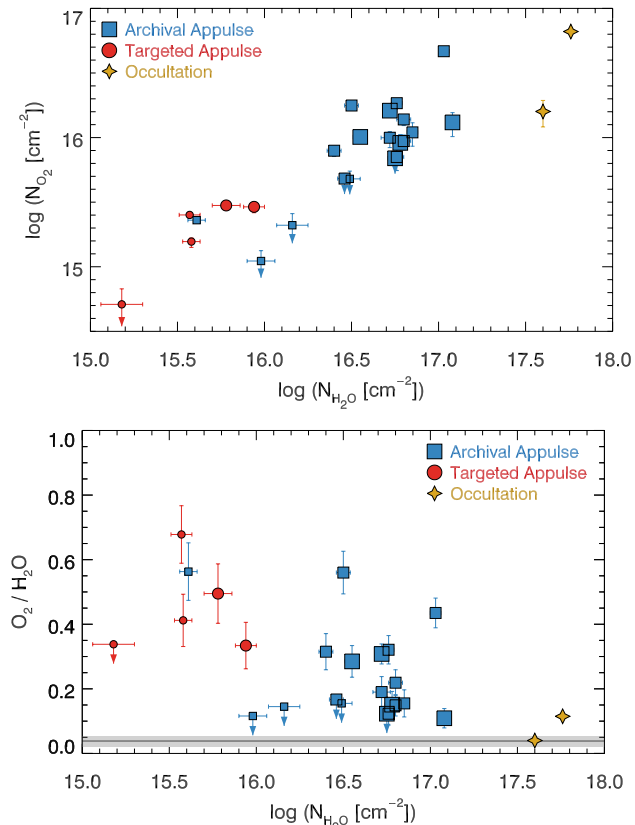


Figure 5. O_2 column density (*top*) and relative abundance of O_2/H_2O (*bottom*) as a function of N_{H_2O} for the two post-occultation exposures of HD 4150 and the stellar appulses of Keeney et al. (2017). There are clear trends of increasing N_{O_2} and decreasing O_2/H_2O with increasing N_{H_2O} . The shaded area in the bottom panel is the 95% (2σ) confidence band for n_{O_2}/n_{H_2O} from Bieler et al. (2015).

discrepancy in O_2/H_2O abundance between Alice and ROSINA measurements remains elusive.

4.1. Empirical Coma Model Comparisons

Hansen et al. (2016) developed an empirical coma model to study the evolution of the H_2O production rate between 2014 June and 2016 May. This model is based on comparisons between ROSINA data and Direct Simulation Monte Carlo models of the 3D neutral gas coma, and corroborated by comparisons with other *Rosetta* instruments (VIRTIS, MIRO, RPC) and ground-based dust measurements. Here we compare the predictions of the Hansen et al. (2016) model with H_2O column densities measured by Alice from stellar appulses and occultations.

Hansen et al. (2016) parameterize the number density, n , of H_2O molecules as

$$n = \frac{fQ}{4\pi r^2 v} \quad (1)$$

where Q is the H_2O production rate, r is the distance from the comet center, v is the gas velocity, and f is an empirical correction factor. When $f = 1$, Equation 1 is equivalent to spherically symmetric radial expansion; otherwise, it accounts for the observed anisotropy in the coma of 67P/C-G (Fougere et al. 2016; Hansen et al. 2016; Läuter et al. 2019). Between the equinoxes (2015 May to 2016 March) the factors Q , v , and f are independent of r (see Tables 1 and 2 of Hansen et al. 2016), so the number density can be integrated to find the column density:

$$\begin{aligned} N &= \frac{fQ}{4\pi v} \int_0^\infty \frac{ds}{r^2(s)} \\ &= \frac{fQ}{4\pi v} \int_0^\infty \frac{ds}{s^2 + r_{sc}^2 - 2sr_{sc} \cos \theta} \end{aligned} \quad (2)$$

where r_{sc} is the distance from the spacecraft to the comet center, θ is the angle of the sight line with respect to the comet center, and $r^2(s)$ is given by the law of cosines. The integration is performed along the line of sight, s , starting from the spacecraft position ($s \equiv 0$).

Prior to the inbound equinox, f is a function of both R_h and r (Hansen et al. 2016) and cannot be separated from the integral. Q and v are defined in Equations 7 and 10 of Hansen et al. (2016), and depend only on heliocentric distance:

$$\begin{aligned} Q(R_h) &= \begin{cases} (2.58 \pm 0.12) R_h^{-5.10 \pm 0.05}, & \text{pre-perihelion} \\ (15.8 \pm 0.9) R_h^{-7.15 \pm 0.08}, & \text{post-perihelion} \end{cases} \\ v(R_h) &= (771.0 - 55.5 R_h) \left(1 + 0.171 e^{-\frac{R_h - 1.24}{0.13}} \right) \end{aligned}$$

where Q has units of 10^{28} molecules s^{-1} and v has units of ms^{-1} .

Figure 6 shows the predicted H_2O column density from Equation 2 compared to Alice and VIRTIS measurements near perihelion. The uncertainty on the model predictions is assumed to be 20% (Hansen et al. 2016). The Alice data are consistent with the predicted values over the full range of column densities measured. Using all data obtained between the equinoxes (all but one data point, see Figure 7), where the assumptions behind Equation 2 are valid, the RMS difference between the Alice measurements and the Hansen et al. (2016) prediction is 0.24 dex.

However, for VIRTIS data (Bockelée-Morvan et al. 2016), the predicted column densities are systematically higher than the measurements. Fougere et al. (2016) had to reduce the H_2O column densities predicted by their model by a factor of four to match the measurements of Bockelée-Morvan et al. (2016). The dot-dashed

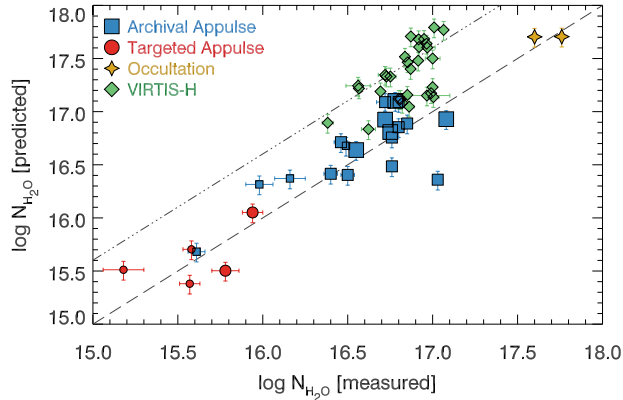


Figure 6. The predicted H_2O column density from Equation 2 compared to Alice and VIRTIS measurements. The dashed line shows perfect agreement between the predicted and measured values, and the dot-dashed line shows predicted values that are four times larger than measured.

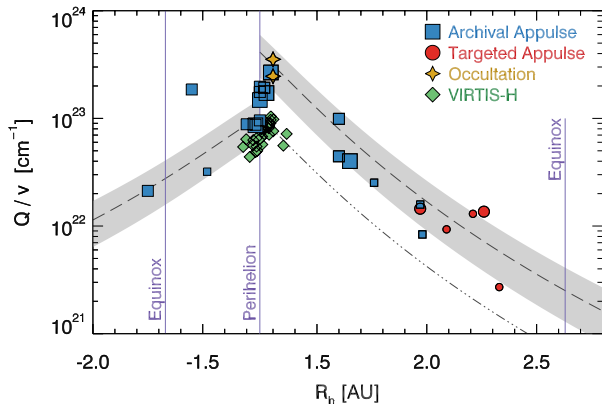


Figure 7. The predicted trend of Q/v as a function of R_h (Hansen et al. 2016), compared to values inferred from Alice and VIRTIS measurements using Equation 3. The shaded region shows the 95% (2σ) confidence band for Q/v and the dashed lines show the best-fit relation from Hansen et al. (2016); the dot-dashed line post-perihelion shows the Hansen et al. (2016) prediction reduced by a factor of four.

line in Figure 6 indicates a model over-prediction by a factor of four and passes through much of the VIRTIS data, agreeing with the analysis of Fougere et al. (2016).

As a final check on the consistency of the Alice data and the Hansen et al. (2016) coma model, Equation 2 can be rearranged so that the details of the observing geometry cancel out, leaving only a predicted trend with heliocentric distance:

$$\frac{Q(R_h)}{v(R_h)} = \frac{4\pi N/f}{\int_0^\infty (s^2 + r_{sc}^2 - 2sr_{sc} \cos \theta)^{-1} ds} \quad (3)$$

Figure 7 shows the Hansen et al. (2016) prediction of Q/v as a function of R_h compared to values derived from

Alice and VIRTIS measurements using Equation 3. The dashed lines show the best-fit relation of Hansen et al. (2016), and the gray shaded regions show the 95% (2σ) confidence band for the prediction. The Alice appulse (Keeney et al. 2017) and occultation measurements (Figure 3-4) are consistent with the Hansen et al. (2016) prediction, except very close to perihelion where the Hansen et al. (2016) model is discontinuous.

The VIRTIS-H data are lower than the Hansen et al. (2016) prediction over the full range of heliocentric distance, and show no discontinuity at perihelion. The disagreement is largest after perihelion, where the VIRTIS data are lower than the prediction by a factor of ~ 4 (dot-dashed line). Fougere et al. (2016) discussed possible reasons for this discrepancy and we will not speculate further, except to note that it is reassuring that we are able to reproduce the reported tension.

Furthermore, the fact that our H_2O measurements are consistent with the predictions of the Hansen et al. (2016) coma model increases confidence in our ability to directly compare results from Alice and ROSINA. On the other hand, the broad consistency in H_2O results between the two instruments makes the discrepancy in $\text{O}_2/\text{H}_2\text{O}$ values all the more puzzling.

4.2. Modeling Uncertainties

There are several sources of systematic uncertainty in our modeling process, as detailed in Keeney et al. (2017). Perhaps the hardest to quantify is the uncertainty introduced by unknown far-UV absorption cross sections. ROSINA-DFMS has found dozens of species in the coma of 67P/C-G (Le Roy et al. 2015; Altwegg et al. 2017), many of which have no measured far-UV cross sections, and could thus conceivably have a large enough cross section that even a trace amount could produce appreciable absorption. We believe this circumstance is unlikely but cannot rule it out.

Another concern is temperature dependence of the adopted cross sections, because all of the cross sections we use were measured at 250-300 K (see Table 3 of Keeney et al. 2017), and the coma is expected to cool adiabatically. There are several reasons for this choice. First, high-resolution laboratory measurements are not consistently available for all modeled species at any other temperature. Adopting a consistent temperature for the cross sections of all modeled species minimizes the uncertainty introduced by cross sections for different species having different behavior with decreasing temperature.

Reassuringly, Figure 6 shows that Alice measurements of H_2O , derived from absorption cross sections measured at 250 K (Chung et al. 2001), are consistent with the predictions of the Hansen et al. (2016) empirical coma

model for 67P/C-G. Thus, if temperature-dependent cross sections are invoked to explain different O_2/H_2O measurements from ROSINA and Alice, they must preferentially affect O_2 or else the Alice and ROSINA H_2O values would disagree.

Finally, and most speculatively, there are O_2 and H_2O cross-section measurements at multiple temperatures over part of the modeled far-UV wavelength range which suggest that using room-temperature cross sections yields lower O_2/H_2O values than at lower temperatures. Low-resolution measurements (Yoshino et al. 2005) indicate that the peak O_2 cross-section at ~ 1400 Å decreases by ~ 0.1 dex as the temperature decreases from 295 to 78 K, implying that a larger O_2 column density is required to match the observed absorption at lower temperatures. High-resolution H_2O cross sections are available at 250 K (Chung et al. 2001) and 298 K (Mota et al. 2005), and the peak cross section at ~ 1650 Å is ~ 0.1 dex larger at 250 K, implying that a smaller H_2O column density is required to match the observed absorption at lower temperatures. Although we cannot be confident that the H_2O cross section continues to increase at temperatures < 250 K, the existing data indicate that lower temperatures necessitate larger O_2/H_2O to fit the data, further suggesting that adopting room-temperature cross sections is not the cause of the discrepancy between our O_2/H_2O values and the ROSINA measurements.

5. SUMMARY

We have presented far-UV spectra of the A0 IV star HD 4150, which was serendipitously observed by *Rosetta*'s Alice imaging spectrometer on 2015 September 13. HD 4150 was observed in two 10-minute integrations immediately after being occulted by 67P/C-G, and revisited approximately 9 months later when its line of sight was far from the nucleus. By comparing the two epochs of stellar spectra, we were able to quantify the amount of H_2O and O_2 within 1 km of the nucleus.

We find that $N_{H_2O} \propto \rho^{-1}$ in our consecutive exposures of HD 4150, but N_{O_2} decreases ~ 3 times faster than N_{H_2O} . We have also measured a value of N_{O_2}/N_{H_2O} that is consistent with ROSINA measurements of n_{O_2}/n_{H_2O} (Bieler et al. 2015; Fougere et al. 2016). Combining our observations of HD 4150 with previous results from Keeney et al. (2017), we confirm the strong correlation between O_2 and H_2O (see top panel of Figure 5, which demonstrates that N_{O_2} increases as N_{H_2O} increases) first

reported by ROSINA (Bieler et al. 2015; Fougere et al. 2016), but find a general decrease in O_2/H_2O with increasing N_{H_2O} in Alice data (see bottom panel of Figure 5), even though the HD 4150 data in isolation suggest otherwise. This trend of decreasing O_2/H_2O with increasing N_{H_2O} partially explains the initial discrepancy in O_2/H_2O between Alice and ROSINA.

Several *Rosetta* instruments (e.g., Alice, ROSINA, VIRTIS, MIRO) can detect H_2O in the coma of 67P/C-G. However, only Alice and ROSINA can directly detect O_2 , so the differing Alice and ROSINA measurements of O_2/H_2O in the coma of 67P/C-G remain mysterious, especially since we have shown that our H_2O measurements are consistent with the empirical coma model of Hansen et al. (2016).

We have investigated several potential sources of this discrepancy, but none have provided a satisfactory explanation. We note, however, that additional high-resolution laboratory measurements of molecular absorption cross sections in the far-UV at temperatures of ~ 100 K would be welcome.

One avenue of future study is modeling the O_2/H_2O distribution throughout the coma of 67P/C-G, then integrating along the Alice line of sight to predict the observed column density ratio. The models of Hansen et al. (2016), Fougere et al. (2016), and Läuter et al. (2019) are based off of *in-situ* ROSINA samples of the coma density and composition, and largely agree with emission-line measurements from MIRO (Biver et al. 2015; Lee et al. 2015), VIRTIS (Bockelée-Morvan et al. 2015; Fink et al. 2016), and Alice (Feldman et al. 2016). However, emission-line intensities are far more sensitive to density than absorption (n^2 compared to n dependence), so a distributed source of O_2 would preferentially reveal itself in absorption.

Rosetta is an ESA mission with contributions from its member states and NASA. We thank the members of the *Rosetta* Science Ground System and Mission Operations Center teams, in particular Richard Moissl and Michael Küppers, for their expert and dedicated help in planning and executing the Alice observations. The Alice team acknowledges continuing support from NASA via Jet Propulsion Laboratory contract 1336850 to the Southwest Research Institute. This research has made use of the SIMBAD database, operated at CDS, Strasbourg, France.

Facility: *Rosetta* (Alice)

REFERENCES

- Altwegg, K., Balsiger, H., Berthelier, J. J., et al. 2017, MNRAS, 469, S130
- Balsiger, H., Altwegg, K., Bochsler, P., et al. 2007, SSRv, 128, 745

- Bieler, A., Altwegg, K., Balsiger, H., et al. 2015, *Nature*, 526, 678
- Biver, N., Hofstadter, M., Gulkis, S., et al. 2015, *A&A*, 583, A3
- Bockelée-Morvan, D., Debout, V., Erard, S., et al. 2015, *A&A*, 583, A6
- Bockelée-Morvan, D., Crovisier, J., Erard, S., et al. 2016, *MNRAS*, 462, S170
- Bockelée-Morvan, D., Rinaldi, G., Erard, S., et al. 2017, *MNRAS*, 469, S443
- Cairns, R. B., & Samson, J. A. R. 1965, *J. Geophys. Res.*, 70, 99
- Chung, C.-Y., Chew, E. P., Cheng, B.-M., Bahou, M., & Lee, Y.-P. 2001, *Nuclear Instruments and Methods in Physics Research A*, 467, 1572
- Coradini, A., Capaccioni, F., Drossart, P., et al. 2007, *SSRv*, 128, 529
- Feldman, P. D., A'Hearn, M. F., Feaga, L. M., et al. 2016, *ApJL*, 825, L8
- Fink, U., Doose, L., Rinaldi, G., et al. 2016, *Icarus*, 277, 78
- Fougere, N., Altwegg, K., Berthelier, J.-J., et al. 2016, *MNRAS*, 462, S156
- Fray, N., & Schmitt, B. 2009, *Planet. Space Sci.*, 57, 2053
- Gasc, S., Altwegg, K., Balsiger, H., et al. 2017, *MNRAS*, 469, S108
- Gerig, S.-B., Marschall, R., Thomas, N., et al. 2018, *Icarus*, 311, 1
- Gulkis, S., Frerking, M., Crovisier, J., et al. 2007, *SSRv*, 128, 561
- Hansen, K. C., Altwegg, K., Berthelier, J.-J., et al. 2016, *MNRAS*, 462, S491
- Haser, L. 1957, *Bulletin de la Societe Royale des Sciences de Liege*, 43, 740
- Kanik, I., Noren, C., Makarov, O. P., et al. 2003, *Journal of Geophysical Research (Planets)*, 108, 5126
- Keeney, B. A., Stern, S. A., A'Hearn, M. F., et al. 2017, *MNRAS*, 469, S158
- Läuter, M., Kramer, T., Rubin, M., & Altwegg, K. 2019, *MNRAS*, 483, 852
- Le Roy, L., Altwegg, K., Balsiger, H., et al. 2015, *A&A*, 583, A1
- Lee, S., von Allmen, P., Allen, M., et al. 2015, *A&A*, 583, A5
- Makarov, O. P., Ajello, J. M., Vattipalle, P., et al. 2004, *Journal of Geophysical Research (Space Physics)*, 109, A09303
- Migliorini, A., Piccioni, G., Capaccioni, F., et al. 2016, *A&A*, 589, A45
- Mota, R., Parafita, R., Giuliani, A., et al. 2005, *Chemical Physics Letters*, 416, 152
- Mumma, M. J., Stone, E. J., Borst, W. L., & Zipf, E. C. 1972, *JChPh*, 57, 68
- Pineau, J. P., Parker, J. W., Steffl, A. J., et al. 2019, *Journal of Spacecraft and Rockets*, 56, arXiv:1711.02811
- Rinaldi, G., Bockelée-Morvan, D., Ciarniello, M., et al. 2018, *MNRAS*, 481, 1235
- Stern, S. A., Slater, D. C., Scherrer, J., et al. 2007, *SSRv*, 128, 507
- Yoshino, K., Esmond, J. R., Sun, Y., et al. 1996, *JQSRT*, 55, 53
- Yoshino, K., Parkinson, W. H., Ito, K., & Matsui, T. 2005, *Journal of Molecular Spectroscopy*, 229, 238